ISSN: 0975-833X

Available online at http://www.journalcra.com

International Journal of Current Research

Vol. 16, Issue, 09, pp.*29957-29964*, September, 2024
DOI: https://doi.org/10.24941/ijcr.47762.09.2024

INTERNATIONAL JOURNAL OF CURRENT RESEARCH

REVIEW ARTICLE

COMPARATIVE STUDY OF 1-D AND 3-D MODELLING OF THE IMPACT OF MAGNETIC FIELD INTENSITY ON THE ELECTRICAL PERFORMANCE OF A BIFACIAL POLYCRYSTALLINE SILICON PV CELL

Idrissa Sourabié[1], Boubacar Soro[2], Alain Doua Gnabahou[2], Mahamadi Savadogo[2], Martial Zoungrana[2] and Issa Zerbo[2]

[1]Laboratoire de Chimie Analytique, de Physique Spatiale et Énergétique (L@CAPSE), Ecole Doctorale, Sciences et Technologies, Université Norbert ZONGO, Koudougou, Burkina Faso; [2]Laboratoire d'Energies Thermiques REnouvelables (L.E.T.RE), Ecole Doctorale Sciences et Technologies, Université Joseph KI-ZERBO, Ouagadougou, Burkina Faso

ARTICLE INFO

Article History:
Received 20th June, 2024
Received in revised form
19th July, 2024
Accepted 19th August, 2024
Published online 30th September, 2024

Key words:
Magnetic Field, Modelling, Bifacial Solar Cell, Multispectral Illumination, Conversion Efficiency.

***Corresponding author:**
Idrissa Sourabié

ABSTRACT

The aim of this work is to carry out a comparative study of the magnetic field effect of 1-D and 3-D modelling on a bifacial polycrystalline silicon solar cell under multispectral illumination from both sides. The continuity equations were solved in order to obtain the expressions for the various electron densities. The expressions for the carrier densities (electrons) were used to obtain the expressions for the electrical parameters, such as photocurrent density (Jph), photovoltage (Vph) and electrical power P. The conversion efficiency, form factor (FF) and resistance at the point of maximum power Rop of the PV cells were then calculated. The results of the simulations showed that except for the currents, which decrease, the other electrical parameters for a 1-D model are greater than those for a 3-D model for each value of magnetic field considered. They also show that the value 2.5mT would be the optimum value for the magnetic field and an average regression rate of 13.25% in the performance of 3-D modelling compared with 1-D. This justifies that the magnetic field alters the one-dimensional case more than the three-dimensional case.

Citation: Idrissa Sourabié, Boubacar Soro, Alain Doua Gnabahou, Mahamadi Savadogo, Martial Zoungrana and Issa Zerbo. 2024. "Comparative study of 1-D and 3-D modelling of the impact of magnetic field intensity on the electrical performance of a bifacial polycrystalline silicon PV cell.*"*. *International Journal of Current Research*, 16, (09), 29957-29964.

INTRODUCTION

The discovery of the solar cell element in 1954 aroused particular interest in the world of research. Researchers such as J. Dugas (1) and B. Ba et al (2) have worked on three-dimensional (3-D) modelling of the PV cell. This modelling makes it possible to carry out a complete study of the solar cell, taking into account its internal parameters. These are: the grain boundaries (GBs) and the recombination speed at the grain boundaries (Sgb). It emerges from their study that the solar cell should be modelled as a regular arrangement of grains of well-defined shape and rectangular form or of the same size as parallelepipeds (3,4) with the same electrical properties as a PV cell. Current research aims to improve the performance of PV cells exposed to external factors. These factors are: temperature, irradiation, humidity, dust, magnetic field, etc. Among these factors, the magnetic field is a factor to be taken into account with regard to industrialisation. This is what first motivated I. Zerbo et al (5)(6) and (7)(8) to investigate the effect of the magnetic field on the electrical performance of a bifacial polycrystalline silicon solar cell in one dimension, and other authors (9)(10)(11)(12) in three dimensions. The various studies show that the magnetic field has a negative effect on the electrical performance of PV modules. However, no study has shown a causal effect between 1-D and 3-D modelling, hence the focus of our study. The aim of this work is to carry out a comparative study between one-dimensional and three-dimensional modelling on the electrical performance of a bifacial polycrystalline silicon solar cell illuminated simultaneously from both sides under an external magnetic field in the static regime. First, we solve the 1-D and 3-D continuity equations leading to the excess minority carrier density. Secondly, the J-V and P-V characteristics are plotted in the same axis system. Finally, the maximum electrical power, form factors and conversion efficiencies are determined directly from the J-V and P-V characteristics and by calculation.

Theoretical study: The study is carried out for the two models (one dimension and three dimensions) on the basis of the n+-p-p+ type polycrystalline silicon (pc-si) bifacial solar cell. The study is carried out in the static regime, taking into account the BSF.

For the 3-D modelling, we consider a parallelepiped-shaped solar cell grain (dimensions gx=gy= 0.003cm) with the same electrical properties as a PV cell.

To ensure the success of our work, the following assumptions must be taken into account:

- The two PV cells are illuminated simultaneously from both sides.
- Light penetration occurs along the axis perpendicular to the junction (Oz), as does the generation of excess minority charge carriers.
- The contribution of the emitter is not taken into account because the dimensions of the base of the photocell along the x and y axes are very large compared with its thickness.
- The crystalline field in the base of the solar cell is assumed to be zero because we are working in quasi-neutral base theory (QNB) (5).
- The grain boundaries are taken perpendicular to the junction and the recombination velocities at the grain boundaries (Sgb) are independent of the depth z and the generation rate for a given illumination. The boundary conditions at the grain boundaries are then linear differential equations with constant coefficients
- The thickness of the base is H = 0.03 cm and the values of the electronic parameters are :
- $Sb = 10^4$ cm.s^{-1} , $Sgb = 10^3$ cm.s^{-1} , Ln = 0.015 cm, $Dn = 26$ cm^2 .s^{-1} (13).
- Magnetic field intensity values are derived from a generating source whose values are greater than those of the Earth's magnetic field.
- The magnetic field is oriented parallel to the junction along the (Oy) axis (5) (6)(9).

The two models of solar cell used in this study and subjected to constant multispectral illumination are shown in Figure 1.

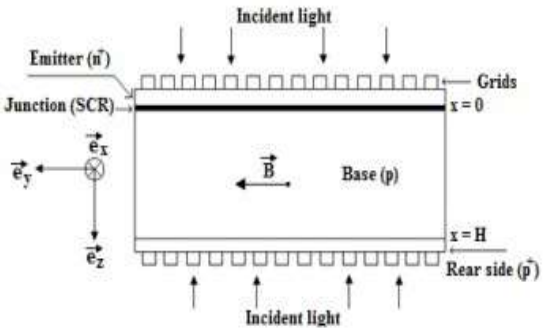

Figure 1. Bifacial silicon solar cell illuminated by multispectral light and under magnetic field influence

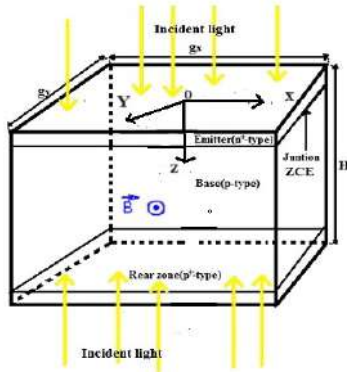

Figure 2. Silicon solar cell grain illuminated by multispectral light and under magnetic field influence

When the two PV cells subjected to a magnetic field are illuminated simultaneously by multispectral light, the continuity equation governing the variation of electrons (electron density in the different bases) is given in equation (1).

$$\frac{1}{e}\vec{\nabla}\cdot\vec{j_n} + G_n(z) - \frac{\delta(n)}{\tau_n} = 0 \qquad (1)$$

$G_n(z)$ represents the rate of generation of electron-hole pairs along the axis (Oz). For double illumination of both sides, its expression is:

$$G_n(z) = \sum_{i=1}^{3} a_i \left(e^{-b_i \cdot x} + e^{-b_i (H-x)} \right) \qquad (2)$$

With a_i and b_i, constants obtained from tabulated values of solar radiation and the wavelength dependence of the absorption coefficient of silicon under standard conditions Air Mass 1.5(14). $\vec{j_n}$ is the electon diffusion current density vector from the base to the junction. Its expression is given in equations (3) and (4).

For double illumination of the solar cell, ai and bi take on the values shown in Table 1.

$a_1=6.13\times10^{20}$	$a_2=0\times54.10^{20}$	$a_3=0\times0991.10^{20}$
$b_1=6630$	$b_2=1000$	$b_3=130$

- In one dimension we have:

$$\overrightarrow{j_n} = eD_n\delta(x) \tag{3}$$

-In three dimensions, we have:

$$\overrightarrow{j_n} = eD_n\delta(x,y,z) \tag{4}$$

Taking equations (3) and (4) as 1-D and 3-D respectively in equation (1), we obtain equations (5) and (6).

$$\frac{\partial^2\delta(x)}{\partial x^2} - \frac{\delta(x)}{L_n^{*2}} + \frac{G(x)}{D_n^*} = 0 \tag{5}$$

$$\frac{\partial^2\delta(x,y,z)}{\partial x^2} + (1+(\mu_n B)^2\frac{\partial^2\delta(x,y,z)}{\partial y^2} + \frac{\partial^2\delta(x,y,z)}{\partial z^2} - \frac{\delta(x)}{L^{*2}} + \frac{G(x)}{D_n^*} = 0 \tag{6}$$

$L_n^{*2} = \tau \cdot D_n^*$ and $L^* = \frac{L_n}{1+(\mu_n B)^2}$ are the diffusion lengths dependent on the magnetic field. The general solutions of partial differential equations (5) and (6) are given in equations (7) and (8) respectively.

$$\delta(x,B) = A \cdot ch\left(\frac{x}{L_n^*}\right) + B \cdot sh\left(\frac{x}{L_n^*}\right) + \sum_{i=1}^{3} k_i\left(e^{-b_i \cdot x} + e^{-b_i(H-x)}\right) \tag{7}$$

$$\delta(x,y,z,B) = \sum_j \sum_k \left[A_{j,k} \cdot ch\left(\frac{z}{L_{j,k}^*}\right) + B_{j,k} \cdot sh\left(\frac{z}{L_{j,k}^*}\right) + \sum_{i=1}^{3} K_i\left(e^{-b_i \cdot z} + e^{-b_i(H-z)}\right)\right] \tag{8}$$

With $k_i = -a_i \cdot \left[D_n^* \cdot \left(b_i^2 - \frac{1}{L_n^{*2}}\right)\right]$ and $K_i = \frac{a_i \cdot L_{j,k}^2}{D_{j,k} \cdot \left[\left(b_i \cdot L_{j,k}\right)^2 - 1\right]}$

Thus the constants A, B, $A_{j,k}$ and $B_{j,k}$ are determined using the boundary conditions at the emitter-base junction ((x= 0) and (Z=0)) and on the back ((x= H) and (z=H)) of the PV cell base (1) (2) (4) (6) (14).

By using Fick's law in one dimension given by (5,6) (equation (9)) and in three dimensions by (12,13) (equation (10)) we obtain the different expressions for the photocurrent density.

$$J_{ph}(Sf,B) = eD_n^* \left.\frac{\partial\delta(x)}{\partial x}\right|_{x=0} \tag{9}$$

$$J_{ph}(Sf,B) = \frac{e \cdot D_n^*}{g_x \cdot g_y} \int_{-\frac{g_y}{2}}^{\frac{g_y}{2}} \int_{-\frac{g_x}{2}}^{\frac{g_x}{2}} \left[\frac{\partial\delta(x,y,z)}{\partial z}\right]_{z=0} dxdy \tag{10}$$

The Boltzmann approximations for one dimension (equation (11)) and three dimensions (equation (12)) give the expressions for the phototensions.

$$V_{ph}(Sf,B) = V_T \cdot \ln\left[N_B \cdot \frac{\delta(0)}{n_i^2} + 1\right] \tag{11}$$

$$V_{ph}(Sf,B) = V_T \cdot \ln\left(1 + \frac{N_B}{n_i^2} \int_{-\frac{g_y}{2}}^{\frac{g_y}{2}} \int_{-\frac{g_x}{2}}^{\frac{g_x}{2}} \delta(x,y,0)dxdy\right) \tag{12}$$

V_T is the thermal voltage (V_T = 26mV at T = 300K), N_B is the doping rate of acceptor atoms in the base (NB = 1016 cm-3) and ni is the concentration of intrinsic carriers at thermodynamic equilibrium ($n_i = 10^{10}$ cm^{-3}).

When exposed to light, the PV cell behaves like a DC current generator Jph(15) with a DC voltage at its terminals Vph. The product of the voltage and the current gives the electrical power delivered by the cell. Equation (13) gives the expression for the electrical power.

$$P(Sf,B) = J_{ph}(Sf,B)\cdot V_{ph}(Sf,B) \tag{13}$$

Considering an incident light of $100mW/cm^2$ under standard AM 1.5 conditions, the expression for the conversion efficiency of the PV cell is given in equation (14). This expression will be used to obtain the conversion efficiency values.

$$\eta(Sf,B) = \frac{P(Sf,B)_{\max}}{100mW/cm^2} \tag{14}$$

Given the values of the open-circuit voltage Vphco and the short-circuit current Jphcc, and using equation (15), we calculate the form factor FF.

$$FF = \frac{P(Sf,B)_{\max}}{V_{phco}\cdot J_{phcc}} \tag{15}$$

$$R_{op} = \frac{V_m}{J_m} \tag{16}$$

RESULTS AND DISCUSSION

Comparison of open circuit and short circuit states: Looking at the expressions for the photovoltage Vph(Sf, B) and photocurrent density Jph(Sf, B), we see that they depend on the parameter Sf, which is the dynamic velocity at the junction. Using the characteristics Vph(Sf,B)=f(Sf) and Jph(Sf,B)=f(Sf), we can graphically determine the values of Sfco and Sfcc for different values of the magnetic field in 1-D and 3-D. These values are given in Table 2.

Table 2. Dynamic velocity at the junction initiating the short circuit and the open circuit for different values of the magnetic field and for simultaneous illumination of both sides of the bifacial solar cell for the two simulations

	B(mT)	0	2.5	5	7.5	10
1D modelling	$Sf_{cc}(cm/s)$	4.786×10^5	2.818×10^5	2.042×10^5	7.586×10^4	3.090×10^4
		0	40.49	57.33	84.14	93.35
	$Sf_{oc}(cm/s)$	66.069	27.542	16.218	6.31	4.677
		0	58.31	75.45	90.44	92.92
3D modelling	$Sf_{cc}(cm/s)$	2.356×10^5	1.105×10^5	6.657×10^4	5.162×10^4	2.398×10^4
		0	53.09	71.74	78.08	89.82
	$Sf_{oc}(cm/s)$	85.202	35.166	19.019	13.848	10.000
		0	58.72	77.67	83.74	88.26

Table 2 shows that the values of the electronic parameters evolve in the same direction as those of the magnetic field intensity for both models. Thus we notice for 1D that when the magnetic field increases the dynamic velocity at the junction initiating the short circuit decreases slowly up to the value B≤5mT and decreases very rapidly for B≥5mT. Also, the dynamic velocity initiating the open circuit has the same characteristics as the dynamic velocity initiating the short circuit. We could therefore say that the value B=5mT is the optimum magnetic field value for one-dimensional modelling. On the other hand, for 3D the dynamic velocities initiating the short-circuit and the open circuit decrease slowly as the magnetic field increases. The results in Table 2 show that the magnetic field precipitates the establishment of the short-circuit and therefore the current by 13% for the one-dimensional model compared with the three-dimensional model. This can be seen from the curves in Figure 2. Furthermore, for the open circuit, we note that the magnetic field precipitates its establishment at around 7% between the 1-D and three dimensional models. By comparing the difference in the regression rates of the dynamic velocity initiating the open circuit, we can see that the optimum value for the magnetic field strength is 5mT for both types of modelling. Figure 2 shows the dynamic velocity curves at the junction initiating the open circuit as a function of the magnetic field for the two types of modelling. We note that as the magnetic field increases, both curves decrease. We also note that for the 1D model, the dynamic speed initiating the open circuit is established very quickly compared with the 3D model, hence the magnetic field precipitates the establishment of the open circuit.

Comparison of the displacement of the operating point of the solar cell

As in 1.), the expression of the electrical power P(Sf, B) depends on the parameter Sf Table 3 shows that as the magnetic field increases, the maximum electrical power and the dynamic speed at the point of maximum power in both models (1D and 3D) decrease. The decrease in dynamic speed at the junction corresponds to a shift in the operating point of the solar cell. Note that the dynamic speed and load resistance move in opposite directions.

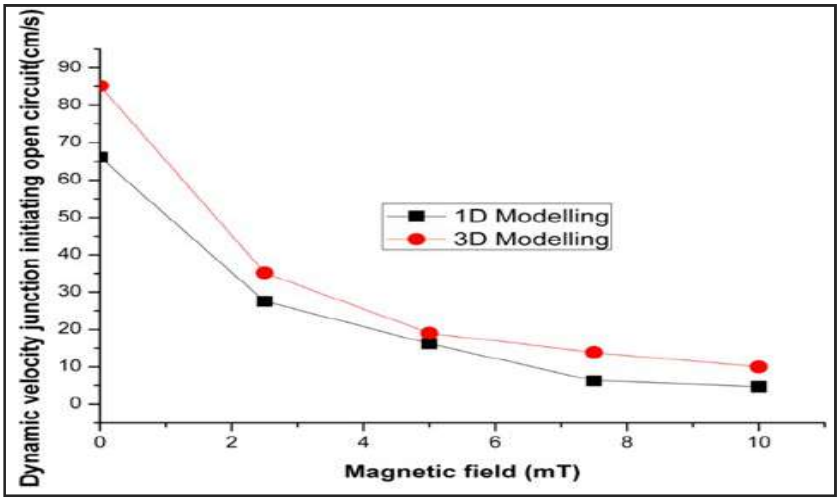

Figure 3. dynamic velocity jonction iniating open circuit function magnetic field

Table 3. Shows the values of Pmax and Sfmax obtained graphically from the plot P(Sf, B)=f(Sf).

	B(mT)	0	2.5	5	7.5	10
1D modelling	$P_{max}(mW/cm^2)$	19.759	16.526	14.776	13.809	13.103
		0	16.36	25.21	30.11	33.68
	$Sf_{Mpp}(cm/s)$	3.020×10^4	1.023×10^4	6.028×10^3	3.981×10^3	3.090×10^3
3D modelling	$P_{max}(mW/cm^2)$	16.056	13.596	12.658	11.969	11.422
		0	15.32	21.16	25.45	28.86
	$Sf_{Mpp}(cm/s)$	1.854×10^4	6.584×10^3	3.903×10^3	3×10^3	1.767×10^3

In other words, when we move towards the open circuit (low dynamic speed) the resistance increases. But when the dynamic speed increases (short-circuit) the load resistance decreases. So the decrease in dynamic speed at the point of maximum power with the increase in the magnetic field corresponds to an increase in load resistance at the point of maximum power (5). Looking at the regression rates for the two models, we see that the 3D regression rate for each given magnetic field value is lower than the 1D regression rate. The dynamic speeds at the point of maximum power show that the operating point of the solar cell for 3D modelling moves further than that for 1D. As a result, the optimum (load) resistance for 3D is smaller than that for 1D. Hence a regression rate of 5% between the two models. This behaviour of the 3D solar cell can be explained by taking all the parameters into account.

Comparison of electrical parameters: The J-V characteristics of the two models are shown in Figure 4a and Figure 4b respectively.

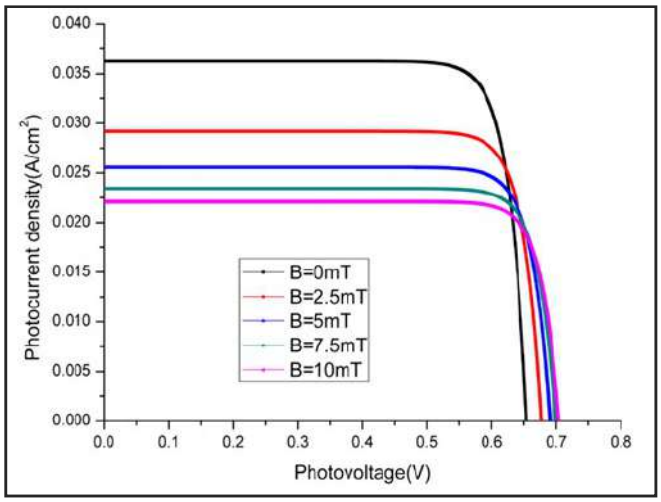

Figure 4a. Photocurrent-photovoltage by 1D modelling

We can see that Figures 4.a and 4.b show the same trends. The currents decrease and the voltages increase as the magnetic field increases. This suggests an accumulation of electrons near the junction. We also observe that for a given value of the magnetic field, the value of the current and voltage for 3D modelling are greater than those for 1D. To obtain the electrical parameters, we used the method proposed by 0. Sow et al(16). This method consists of determining the operating point of the solar cell by constructing the J-V and P-V characteristics in the same system of axes. This method is shown in Fig. 4. Based on this method, Table 4 shows the electrical parameters extracted and those calculated.

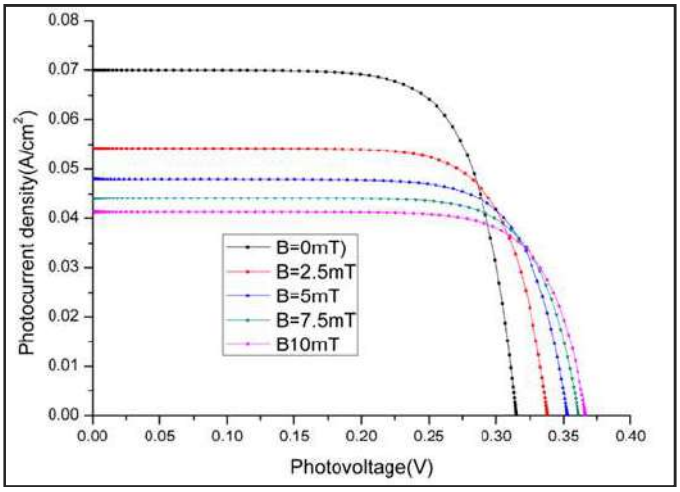

Figure 4b. Photocurrent-photovoltage by 1D modelling

Tableau 4. Electric's parameters for 1 D modeling

	B(mT)	0	2.5	5	7.5	10
1D modelling	$V_m(mV)$	569.76	591.82	604.35	613.89	620.25
	$J_m(mA.cm^{-2})$	34.679	27.924	24.448	22.495	21.125
	$V_{oc}(mV)$	653.87	676.37	689.89	697.71	704.19
	$J_{sc}(mA.cm^{-2})$	36.272	29.183	25.507	23.512	22.095
	FF	0.833	0.837	0.839	0.841	0.842
	$R_{OP}(\Omega.cm^2)$	16.429	21.194	24.719	27.290	29.360
	$P_{max}(mW.cm^{-2})$	19.759	16.526	14.775	13.810	13.103
	$\eta(\%)$	19.759	16.526	14.775	13.810	13.103

Tableau 5. Electric's Parameters for 3D modeling

	B(mT)	0	2.5	5	7.5	10
3D modelling	$V_m(mV)$	264.17	288.09	305.37	310.37	315.59
	$J_m(mA.cm^{-2})$	55.50990	49.2510	43.7530	40.7670	38.2620
	$V_{oc}(mV)$	328.84	355.78	370.59	378.96	384.73
	$J_{sc}(mV)$	60.076	53.184	47.628	43.904	41.139
	FF	0.736773	0.749875	0.756977	0.760494	0.762917
	$R_{OP}(\Omega.cm^2)$	4.79446	5.84942	6.97940	7.613265	8.24813
	$P_{max}(mW.cm^{-2})$	14.555	14.189	13.361	12.653	12.075
	$\eta(\%)$	14.555	14.189	13.361	12.653	12.075

The results in Tables 4 and 5 show that for both models, electrical parameters such as maximum voltage (Vm) and open circuit voltage (Voc) increase with the magnetic field. Meanwhile, the maximum current (Jm) and the short-circuit current (Jsc) decrease as the magnetic field increases. So for both models we see a decrease in maximum electrical power. This decrease in maximum electrical power causes the point of maximum power to shift with the magnetic field towards higher voltage values, resulting in an increase in load resistance. Comparing the voltages of the two models, we can see that the one-dimensional voltages are higher than the three-dimensional voltages as the magnetic field increases. The proportionality ratio between the two models is therefore approximately 2. In other words, an average regression rate of 50%. This means that we have more accumulation of carriers close to the junction for the one-dimensional model than for the three-dimensional model.

If we look at the resistance values at the point of maximum power in Tables 4 and 5, we can see that as each value of magnetic field increases, the values for one dimension are higher than those for three-dimensional modelling. This very significant difference shows that for a one-dimensional model, a great deal of resistance is required to protect the junction from possible destruction due to the accumulation of carriers within it. We also note that when the magnetic field increases, the form factors (FF) of the two models increase by around 10%. Comparing the two, we find an average regression rate of 10.13%. The conversion efficiencies decrease as the magnetic field increases. The behaviour of the conversion efficiencies is shown in Figure 5. We can see that the two curves have the same appearance. However, the curve for one dimension is lower than that for three dimensions. This is justified by the fact that all the manufacturing parameters of the (3D) solar cell have been taken into account, rather than the 1D parameters. The regression rate of the yields is therefore around 13.25%.

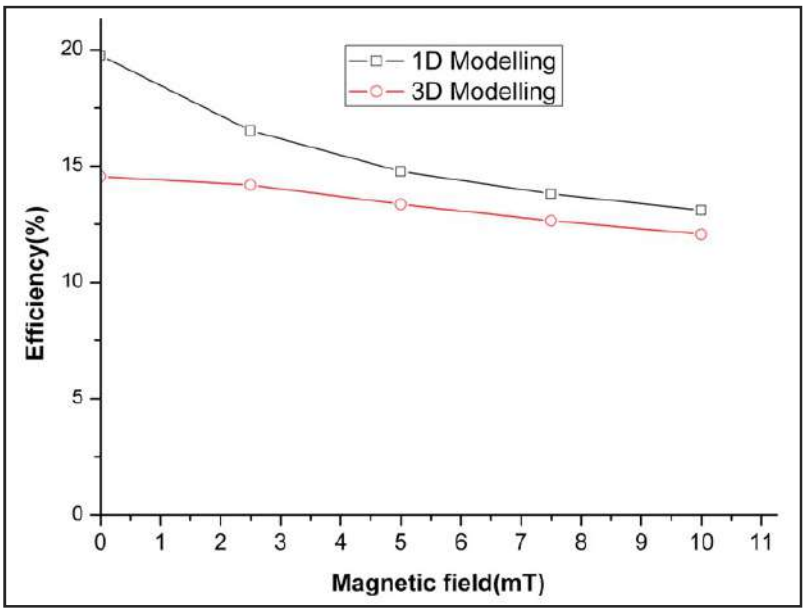

Figure 5. Efficiency an function of magnetic field

CONCLUSION

This work compared the effect of the magnetic field for one-dimensional and three-dimensional modelling on a bifacial polycrystalline silicon solar cell under multispectral illumination from both sides. The study shows that the magnetic field alters the electrical performance of the solar cell more for a one-dimensional model than for a three-dimensional model. This could be explained by the difference in model sizes. The study also showed that the optimum value for the magnetic field is around 2.5mT. At this value, the parameters undergo a sudden increase or decrease.

ACKNOWLEDGEMENTS

The authors are grateful to International Science Program (ISP) for supporting their research group (energy and environment) and allowing them to conduct this work.

Conflicts of Interest: The authors declare no conflicts of interest regarding the publication of this paper.

RÉFÉRENCES

1. Dugas, J. “3D modelling of a reverse cell made with improved multicrystalline silicon wafers,” Solar Energy Materials and Solar Cells, vol. 32, no. 1, pp. 71–88, 1994.
2. Ba B. and M. Kane, “Open-circuit voltage decay in polycrystalline silicon solar cells,” Solar Energy Materials and Solar Cells, vol. 37, no. 3-4, pp. 259–271, 1995.
3. Zouma, B.A.S. Maiga, M. Dieng, F. Zougmoré, and G. Sissoko. 3D approach of spectral response for a bifacial silicon solar cell under a constant magnetic field. Global Journal of Pure and Applied Sciences, 15(1) :117–124, 2009.
4. Zoungrana, M. I. Zerbo, A. Séré, B. Zouma, and F. Zougmoré. 3D study of bifacial silicon solar cell under intense light concentration and under external constant magnetic field. Global Journal of Energineering Research, 10 :113–124, 2011.
5. Zerbo, I. M. Zoungrana, I. Sourabié, A. Ouédraogo, B. Zouma, and D.J. Bathiébo. External magnetic field effect on bifacial silicon solar cell’s electric power and conversion efficiency. Turkish Journal of Physics, 39 :288–294, 201.
6. Zerbo, I. M. Zoungrana, I. Sourabié, A.Ouédraogo, B.Zouma, and D.J. Bathiébo. External magnetic field effect on bifacial silicon solar cell’s electrical parameters. Energy and Power Engineering, 8 :146–151, 2016.
7. Zoungrana, M.I.Zerbo, B.Soro, M.Savadogo, S.Tiendrebeogo, and D.J.Bathiebo. The effect of magnetic field on the efficiency of a silicon solar cell under an intense light concentration. Advances in Science and Technology Research Journal, 11(2) :133–138, 2017.
8. Combari, D.U. I. Zerbo, M.Zoungrana, E.W. Ramdé, and D.J. Bathiebo. Modelling study of magnetic field effect on the performance of a silicon photovoltaic module. Energy and Power Engineering, 9 :419–429, 2017.
9. Madougou, S. F. Made, and M.S. Boukary andG.Sissoko. I–V characteristics for bifacial silicon solar cell studied under a magnetic field. Advanced Materials Research, 18-19 :303–312, 2007.
10. Diaw, M. B. Zouma, A. Séré, S. Mbodji, A. Gueye, and G. Sissoko. 3D study to improve the iqe of the bifacial polycrystalline silicon solar cell from the grain’s geometries and the applied magnetic field. International Journal of Energineering Science and Technology, 4 :3673–3681, 2012.

11. Samb, M.L. M. Zoungrana, R. Sam, M.M. Dione, M.M. Deme, and G. Sissoko. Etude en modélisation à 3–D d'une photopile au silicium en régime statique placée dans un champ magnétique et sous éclairement multispectral : Détermination des paramètres électriques. Journal des Sciences, 10(4) :23–38, 2010.
12. Madougou Nzonzolo, S. S. Mbodji, F.I. Barro, and G. Sissoko. Bifacial silicon solar cell space charge region width determinaion by a study in modelling : effect of the magnetic field. Journal des Sciences, 4(3) :116–127, 2004.
13. Zoungrana, M. M. Thiam, A. Dioum, S. Raguilnaba, and G. Sissoko. 3D study of bifacial silicon solar cell under intense light concentration and under external constant magnetic field : recombination and electric parameters determination. Proceedings of the 22nd European Photovoltaic Solar Energy Conference(Milan), pages 447–453, 2007.
14. Ramatou Saré , Mamoudou Saria , Dioari Ulrich Combari , Idrissa Sourabié, Vinci De Dieu Bokoyo Barandja , Martial Zoungrana , and Issa Zerbo « 3D modelling of the effects of electrons losses at the junction of a polycrystalline silicon PV cell on its performance »
15. International Journal of Innovation and Applied Studies ISSN 2028-9324 Vol. 40 No. 4 Oct. 2023, pp. 1515-1530 © 2023 Innovative Space of Scientific Research Journals http://www.ijias.issr-journals.org/
16. Zerbo, I. M. Zoungrana, A. D. Seré, F. Ouédraogo, R. Sam, B. Zouma, F. Zougmoré « Influence d'une onde électromagnétique sur une photopile au silicium sous éclairement multispectral en régime statique » Revue des Energies Renouvelable vol. 14 N°3(2011) 517-532.
17. Alshushan M. A. S. and I.M. Saleh, «Power degradation and performance evaluation of PV modules after 31 years of work,» In: 2013 IEEE 39th photovoltaic specialists conference (PVSC), Tampa, Florida, USA, pp. 2977-2982, 2013.
18. Sow, O. I. Zerbo, S. Mbodji, M.I. Ngom, M.S. Diouf, G .Sissoko, 2012. Silicon solar cell under electromagnetic waves in steady state : Electrical parameters determination using the I-V and P-V characteristics. International journal of science, environment and technology, vol.1, No 4, 230-246.

****